Direction of Cell Deformation During Microgap Passage

Shigehiro HASHIMOTO
Biomedical Engineering, Department of Mechanical Engineering, Kogakuin University
shashimoto@cc.kogakuin.ac.jp Tokyo, 163-8677, Japan

Sakyo SHIMADA
Biomedical Engineering, Department of Mechanical Engineering, Kogakuin University
Tokyo, 163-8677, Japan

Shogo UEHARA
Biomedical Engineering, Systems Design, Kogakuin University
Tokyo, 163-8677, Japan

ABSTRACT

A biological cell can pass through a narrow gap. The gap plays a role of filter of cells *in vivo*. In the preset study, deformation of a cell during passing through a micro-gap in a micro flow channel has been analyzed *in vitro*. A gap with the rectangular cross section (7 μm high, 0.4 mm wide, and 0.1 mm long) has been made at the middle part of the micro flow channel by the photolithography technique. Myoblasts (C2C12: mouse myoblast cells) were used in the test. The flow rate of the medium fluid, in which cells were suspended, was controlled by the pressure head between the inlet and the outlet. The deformation of each cell passing through the micro gap was observed with an inverted phase-contrast microscope. The experimental results show that the cell tends to extend in the direction of flow with the increase of the velocity during the movement of passing through the gap.

Keywords: Biomedical Engineering, Myoblast, Movement, Deformation, Photolithography and Micro-gap.

1. INTRODUCTION

The deformation of the biological cell relates to the biological function. Several types of the cells can pass through the narrow slit *in vivo*. A red blood cell has a high flexibility to pass through the micro capillary in the blood circulation system *in vivo* [1]. The red blood cell passes through the capillary, of which the dimension is smaller than the diameter of itself. It deforms from the biconcave disk shape to the parachute like shape, when it is passing through the capillary. In the shear field, the red blood cell rotates and deforms to the ellipsoidal shape. The sublethal damage [2] were also detected in the shear flow in the previous studies *in vitro*. Several systems sort cells according to the deformability *in vivo*. A slit is one of the systems, which sorts biological cells *in vivo*. Some cells are able to pass through a very narrow slit.

A photolithography technique [3] enables manufacturing micro grooves [4] or micro-structures [5] in the flow-channel for cell tests *in vitro*. The technique also has been applied to handle cancer cells in diagnostics *in vitro* [6-10]. The gap between micro cylinders was made to sort cells in the previous study [11].

The deformation of the depth direction between cylinders, however, cannot be observed by the conventional optical microscope. To observe the deformed cell at the direction perpendicular to the walls of the gap, another type of the gap is designed with the combination of the micro ridge and groove in the previous study [12]. In the preset study, deformation of a cell during passing through a micro-gap in a micro flow-channel has been analyzed *in vitro*.

2. METHODS

Micro Gap

The gap (0.4 mm wide, 0.1 mm long, 7 μm high) has been designed between a transparent polydimethylsiloxane (PDMS) plate and a borosilicate glass (Tempax) plate. The upper plate of PDMS has a rectangular groove (0.03 mm deap, 0.6 mm wide, 16 mm long) separated in to two half parts with the interval of 0.1 mm length. The lower plate of glass has a rectangular groove (7 μm deap, 0.4 mm wide, 1 mm long). These plates keep contact to make a gap between them. The gap is located at the middle part of the flow channel. The cross-sectional area of the flow channel changes from (0.037 mm × 0.4 mm = 0.0148 mm^2) to (0.007 mm × 0.4 mm = 0.0028 mm^2) at the entrance of the gap.

Mold for Upper Plate

A glass plate was used for a surface mold for the upper disk. The plate was cleaned by an ultrasonic cleaner with alkaline solution for ten minutes and rinsed by the ultrapure water for ten minutes. The surface of the glass plate was hydrophilized by the oxygen plasma ashing for ten minutes at 200 W by the reactive ion etching system. The negative photoresist material of high viscosity (SU8-10: Micro Chem Corp., MA, USA) was coated on the glass plate at 1000 rpm for 30 s with a spin coater. After the photoresist was baked on the heated plate at 338 K for five minutes, the plate was baked on the heated plate at 368 K for ten minutes. The photomask was mounted on the surface of SU8-10, and the photoresist was exposed to the UV light through the mask in the mask aligner (M-1S, Mikasa Co. Ltd., Japan). After the photoresist was baked on the heated plate at 338 K for one minute, the plate was baked on the heated plate at 368 K for five minutes. The photoresist was developed with SU-8 developer (Nippon Kayaku Co., Ltd, Tokyo, Japan) for ten minutes. The glass surface with the micro pattern was rinsed with IPA (2-propanol, Wako Pure Chemical Industries, Ltd.) for five minutes, and with the ultrapure water. The plate was dried by the spin-dryer. The Photoresist was baked on the heated plate at 368 K for three minutes.

ISBN: 978-1-950492-61-9
ISSN: 2771-5914

https://doi.org/10.54808/IMCIC2022.02.17

Upper Plate
After the mold of the glass plate was enclosed with a peripheral wall of polyimide, PDMS (Sylgard 184 Silicone Elastomer Base, Dow Corning Corporation) was poured together with the curing agent on the mold. The volume ratio of curing agent is ten percent of PDMS. After degassing, PDMS was baked at 373 K for one hour in an oven. The baked plate of PDMS is exfoliated from the mold. Two holes of 3 mm diameter were machined with a punching tool at the upper disk to make the inlet and the outlet for the flow channel.

Lower Plate
A glass plate was used for a surface for the lower disk. The plate was cleaned by an ultrasonic cleaner with alkaline solution for ten minutes and rinsed by the ultrapure water for ten minutes. The surface of the glass plate was hydrophilized by the oxygen plasma ashing for ten minutes at 200 W by the reactive ion etching system. The negative photoresist material of high viscosity (SU8-5) was coated on the glass plate at 1400 rpm for 30 s with a spin coater. After the photoresist was baked on the heated plate at 338 K for two minutes, the plate was baked on the heated plate at 368 K for five minutes. The photomask was mounted on the surface of SU8-5, and the photoresist was exposed to the UV light through the mask in the mask aligner (M-1S). After the photoresist was baked on the heated plate at 338 K for one minute, the plate was baked on the heated plate at 368 K for two minutes. The photoresist was developed with SU-8 developer for two minutes. The dimension of the depth of the groove was confirmed by the stylus of the contact profilometer (Dektak XT-E, Bruker Corporation).

Flow Channel
The lower plate with the micro pattern was rinsed with IPA (2-propanol), and with the ultrapure water. The plate was dried by the spin-dryer. The surface of the plate was exposed to the oxygen plasma ashing for one minute by RIE-10NR. The plate was rinsed with Aminopropyltriethoxysilane (APTES) for ten minutes, and with the ultrapure water. After the plate was dried, the upper plate was adhered on the lower plate. The plates were baked in the oven at 368 K for ten minutes.

Flow Test
C2C12 (passage < 10, mouse myoblast cell line originated with cross-striated muscle of C3H mouse) was used in the test. Cells were cultured in advance with the D-MEM (Dulbecco's Modified Eagle's Medium) containing 10% FBS and 1% of Antibiotic-Antimycotic (penicillin, streptomycin and amphotericin B, Life Technologies) in the incubator for one week.

Just before the flow test, the cells were exfoliated from the bottom of the culture dish with trypsin and suspended in the culture medium (1000 cells/cm^3). Before flow test, the flow channel was hydrophilized by the oxygen plasma ashing for one minute by RIE-10NR. The bovine serum albumin solution was prefilled in the flow channel and incubated for ten minutes at 310 K in the incubator.

The suspension of the cells was poured at the inlet of the flow channel (Fig. 1). The small reservoir (the depth of 3 mm and the diameter of 5 mm) at the inlet keeps the pressure head. The suspension flows by the pressure head of 2.5 mm, which makes the pressure difference of 25 Pa between the inlet and the outlet. The flow rate decreases gradually with the decrease of the pressure head. The behavior of cells near the slit was observed with an inverted phase-contrast microscope (IX71, Olympus Co., Ltd., Tokyo) at 298 K (Fig. 2).

The microscopic movie images of thirty frames per second at the shutter speed of 1/2000 s were captured by a camera (DSC-RX100M4, Sony Corporation, Tokyo, Japan).

At the video image, x coordinate was defined as the direction parallel to the flow, and y coordinate was defined as the direction perpendicular to the flow (Fig. 3). In the video image, the direction of flow was from left to right. The position of the left edge of the video image was defined as $x = 0$. At the two-dimensional image, the contour of each cell was traced and analyzed by "ImageJ". The projected two-dimensional area (S) of each cell was calculated. At the contour, the projected length of flow direction (Δx) and projected length of direction perpendicular to flow (Δy) were measured. The deformation direction ratio (D) was calculated by Eq. (1).

$$D = (\Delta x - \Delta y)/ (\Delta x + \Delta y) \quad (1)$$

At the circle, $D = 0$. As the ellipse is elongated to x direction, D approaches to 1. As the ellipse is elongated to y direction, D approaches to – 1.

The contour was approximated to the ellipse (Fig. 2). On the ellipse, the length of the major axis (a), and the length of the minor axis (b) were measured (Fig. 3). The ratio of axes is calculated as the shape index (P) by Eq. (2).

$$P = 1 - b / a \quad (2)$$

At the circle, $P = 0$. As the ellipse is elongated, P approaches to 1. The centroid of the ellipse was used to track the velocity of the cell.

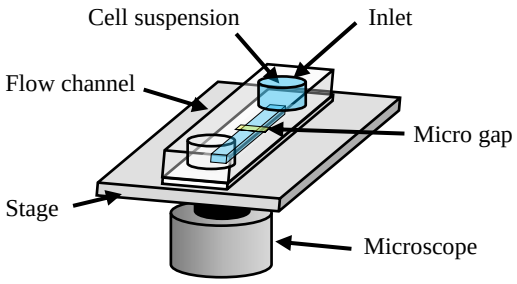

Fig. 1: Flow was generated by pressure head at the inlet, and behavior of cell passing through gap was observed by microscope.

Fig. 2: Contour of two-dimensional projected image of cell was traced; dimension from left to right, 0.1 mm.

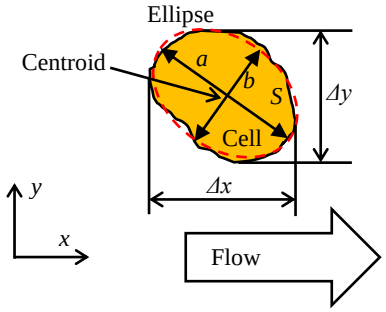

Fig. 3: Contour of two-dimensional projected image of cell was approximated to ellipse. Major axis (*a*), minor axis (*b*), projected length of flow direction (*Δx*), and projected length of direction perpendicular to flow (*Δy*) were measured.

3. RESULTS

A cell stops at the stepped wall of the gap before entering the gap. Several cells pass through the gap in a few seconds. Figs. 4 and 5 exemplify the typical behavior of a cell in the micro gap. Fig. 4 shows relationships between each parameter and time (*t*). Fig. 5 shows relationships between each parameter and position (*x*). Figs. 4a and 5a show tracings of the velocity of the cell (*v*). Figs. 4b and 5b show tracings of the two-dimensional projected area of the cell (*S*). Figs. 4c and 5c show tracings of the shape index of the cell (*P*). Figs. 4d and 5d show the deformation direction ratio of the cell (*D*).

When the cell stops at the gap inlet position at 800 µm, the velocity of the cell drops sharply (Fig. 4a). When the cell leaves the gap at 1000 µm, the velocity (*v*) of the cell increases sharply. In the gap, the velocity of the cell fluctuates intermittently. The two-dimensional projected area (*S*) of the cell increases gradually from 920 µm to 1000 µm in the gap (Fig. 4b). The shape index (*P*) of the cell fluctuates every time regardless of the gap (Fig. 4c). For non-spheres, the shape index (*P*) of the two-dimensional projection plane changes not only with deformation but also rotation. The shape index (*P*) fluctuates over the wider range between 0 and 0.2 out of the gap mainly with rotation of the cell. Outside the gap, the shape index (*P*) fluctuates over a wider range between 0 and 0.2. In the gap between 800 µm to 1000 µm, the shape index (*P*) varies in the narrower range around 0.1. Outside the gap, the deformation direction ratio (*D*) fluctuates between 0 and 0.1. In the gap between 800 µm to 1000 µm, the deformation direction ratio (*D*) varies between – 0.1 and 0.1. The cell stops in the gap from 0.8 s to 1.3 s (Fig. 5a) with the maximum value (800 µm^2) of the two-dimensional projected area (*S*) (Fig. 5b). During the stop, the two-dimensional shape of the cell approaches to circle ($P \approx 0$, $D \approx 0$) (Figs. 5c and 5d). Before stopping in the gap, the cell deforms perpendicular to the flow direction from 0.3 s to 0.8 s (Fig. 5d) with the maximum value of the shape index of 0.3 at 0.5 s (Fig. 5c) in the gap. Fig. 6a shows the relationships between the shape index (*P*) and the two-dimensional projected asea (*S*) of the cell while passing through the gap. The shape index (*P*) tended to approach to zero, which corresponds to the circle, as the area (*S*) increases. Fig. 6b shows the relationships between the deformation direction ratio (*D*) and the shape index (*P*) of the cell while passing through the gap. The deformation direction ratio (*D*) tends to increase with the shape index (*P*) of cell. The cell tends to extend in the direction of flow in the gap. Fig. 6c shows the relationships between the shape index (*P*) and the velocity (*v*) of the cell while passing through the gap. The shape index tends to increase with the increase of the velocity of the cell. Fig. 6d shows the relationships between the deformation direction ratio (*D*) and the velocity (*v*) of the cell while passing through the gap. The deformation direction ratio tends to increase with the increase of the velocity of the cell. The cell tends to extend in the direction of flow with the increase of the velocity in the gap.

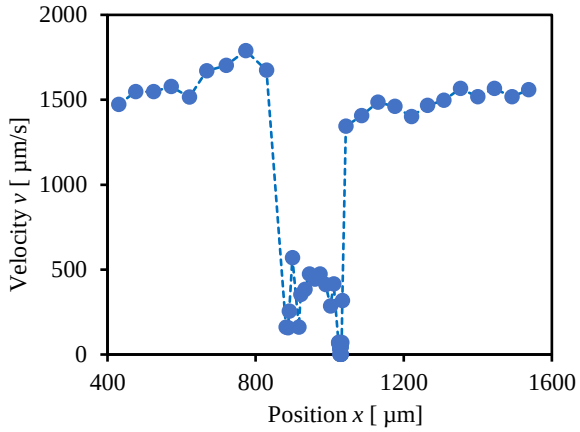

Fig. 4a: Relation between velocity (*v*) and position (*x*) of cell (No. 12).

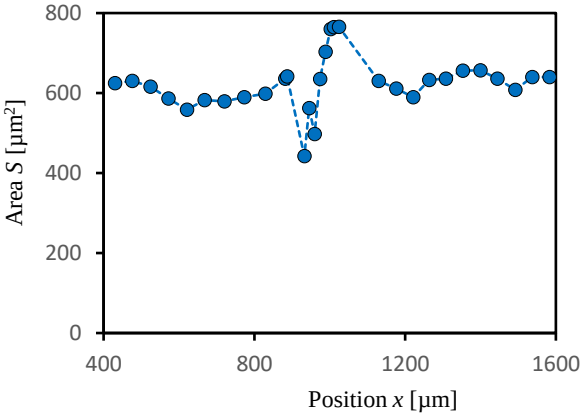

Fig. 4b: Relation between area (*S*) and position (*x*) of cell (No. 12).

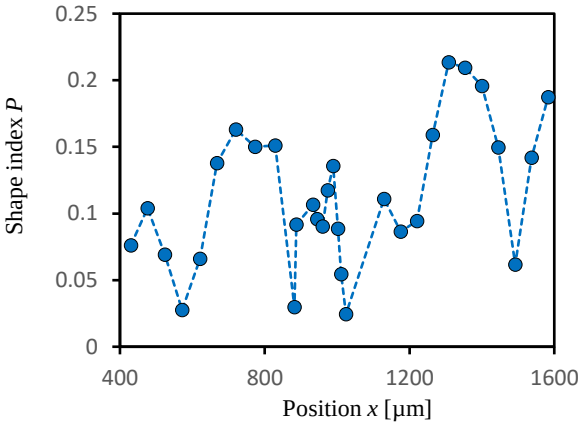

Fig. 4c: Relation between shape index (*P*) and position (*x*) of cell (No. 12).

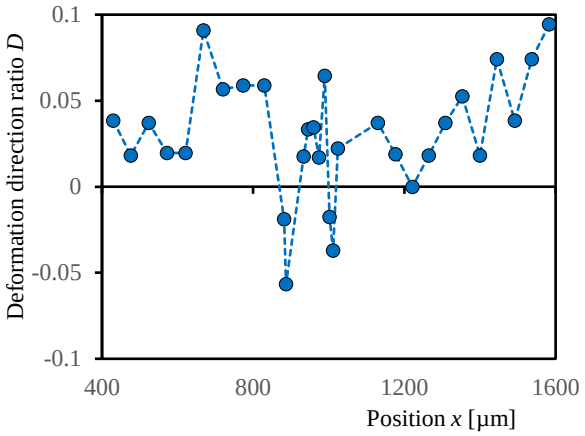

Fig. 4d: Relation between deformation direction ratio (*D*) and position (*x*) of cell (No. 12).

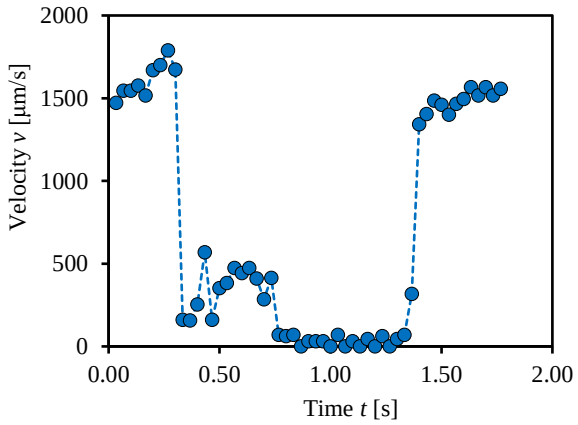

Fig. 5a: Velocity (*v*) tracings of cell (No. 12).

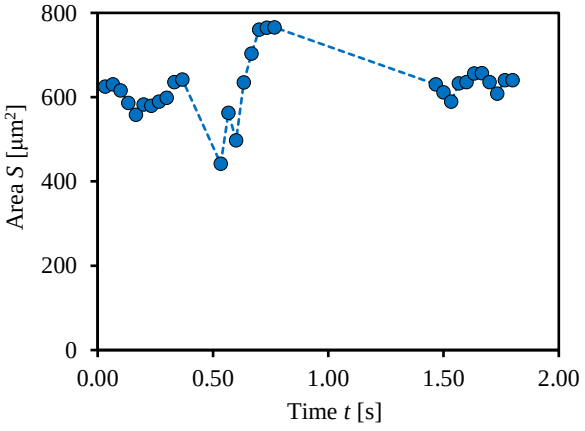

Fig. 5b: Area (*S*) tracings of cell (No. 12).

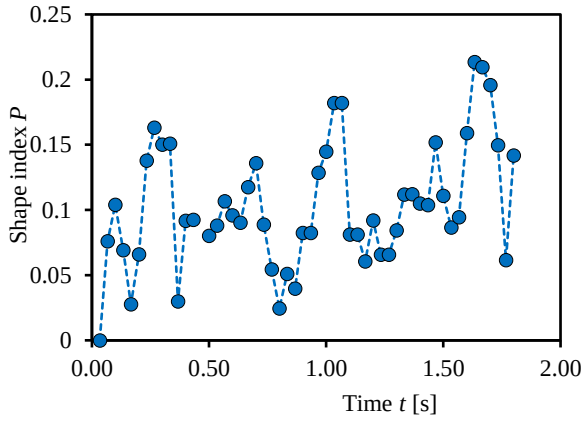

Fig. 5c: Shape index (*P*) tracings of cell (No. 12).

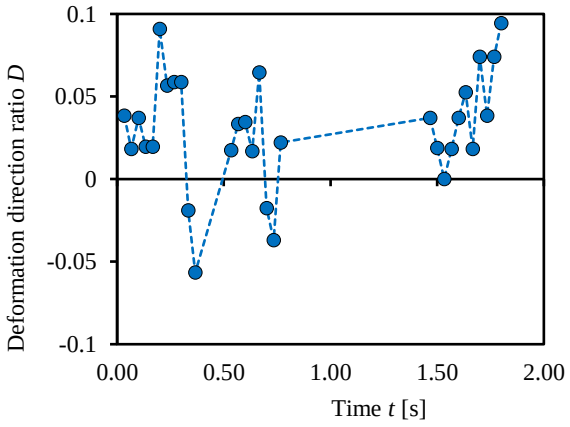

Fig. 5d: Deformation direction ratio (*D*) tracings of cell (No. 12).

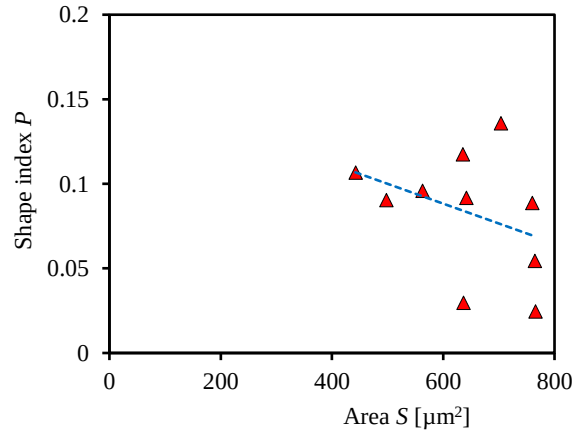

Fig. 6a: Relationship between shape index (*P*) and asea (*S*) of cell (No. 12) while passing through gap. $D = -1\times10^{-4}\ S + 0.16$, $r = 0.36$.

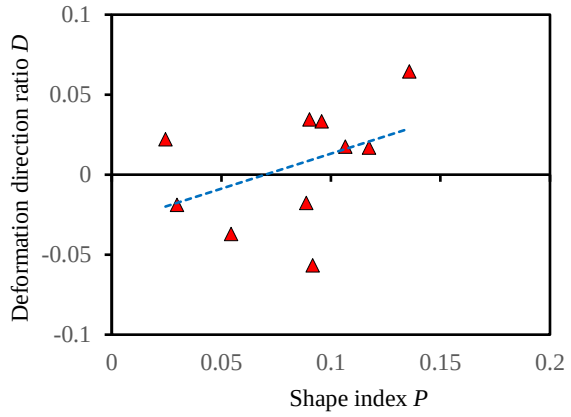

Fig. 6b: Relationship between deformation direction ratio (D) and shape index (P) of cell (No. 12) while passing through gap. $D = 0.44\ P - 0.03$, $r = 0.43$.

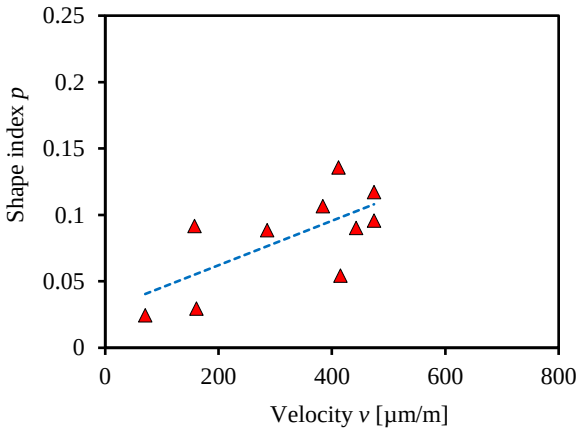

Fig. 6c: Relationship between shape index (P) and velocity (v) of cell (No. 12) while passing through gap. $P = 2\times10^{-4}\ v + 0.03$, $r = 0.68$.

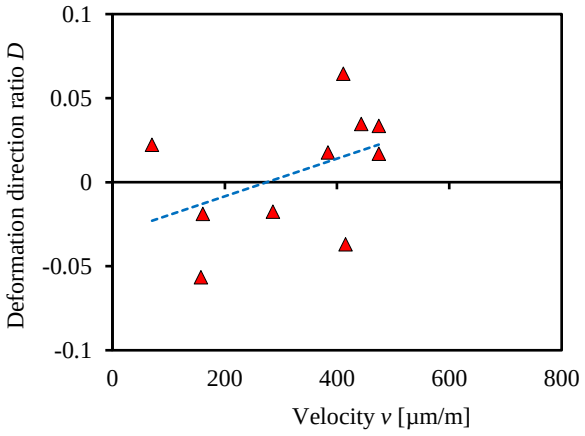

Fig. 6d: Relationship between deformation direction ratio (D) and velocity (v) of cell (No. 12) while passing through gap. $D = 1\times10^{-4}\ v - 0.03$, $r = 0.45$.

4. DISCUSSION

Reynolds number (Re) is calculated by Eq. (3).

$$Re = \rho\ v\ w/\ \eta \tag{3}$$

In Eq. (3), ρ is the density of the fluid, v is the velocity of the flow before the slit, w is the width of the channel before the slit, and η is the viscosity. Re is 1, when ρ, v, w, and η are 10^3 kg m^{-3}, 2×10^{-3} m/s, 6×10^{-4} m, and 1×10^{-3} Pa s, respectively. The turbulent flow does not occur in the flow of this level of small value of Reynolds number.

For the reason of the limitation of the present micromachining technique with the photolithography process, the edge of the ridge is not sharp. The edge has a certain width. The biological system might have the sharper edge, so that a cell passes easily through the slit with the shorter travel distance *in vivo* [1]. The cell has to struggle to pass through the gap in the present experimental device with the longer travel distance.

The moving velocity of the cell suspended in the medium follows the medium velocity. In the previous study [13], the flow rate was controlled by the syringe pump. In that case, the flow rate varied because of several factors: the compliance of the wall of the flow path and clogging of the flow path. The flow rate is controlled by the pressure difference between inlet and outlet of the flow channel in the present study, which has advantage to keep the inner pressure of the flow channel for the morphological stability of the flow channel. The moving velocity also depends on the interaction between the cell and the surface of the gap. To keep the surface property of the channel stable, bovine serum albumin is pre-coated on the surface of the flow path by prefilling the bovine serum albumin solution in the channel in the present study.

The deformability of the biological single cell depends on several factors [7]. The deformability has been analyzed in several studies: using microfluidics [5], measuring local viscoelasticity [14], using atomic force microscopy [15], and using cell mechanics model [16]. The methodology can also be applied to the soring technology on cells [17]. The deformation in the gap is evaluated with the ratio of the projected area of the plan view of the disk-like shape during passing through the gap in the present study. The deformation in the perpendicular direction can be observed at another type of the gap: between micro cylindrical pillars [11].

In the previous study, the projected area of the myoblast cell approaches a circle in the gap when the major axis is parallel to the flow [18]. Cells with a projected area more than 1000 μm^2 tended to stop in the gap (7 μm high). In the present study, Cells with a projected area of approximately 600 μm^2 were selected to track the movement of the single cell. Particles of the diameter smaller than 7 μm can pass through the gap with higher velocity. The ratio of the cross-sectional area between the flow channel (0.0148 mm^2) and the gap (0.0028 mm^2) is 5. Using continuity of the fluid, the mean flow velocity of the medium in the gap is 5 times faster than that before the gap.

In the present study, the shape index (P) fluctuates in a wider range from 0 to 0.2 outside the gap, primarily with cell rotation (Fig. 4c). In the gap between 800 μm to 1000 μm, the shape index (P) varies in the narrower range around 0.1, mainly due to cell deformation. In the present test, every myoblast cell is forced to be deformed, when the cell is passing through the gap with the

height of 7 μm. The nucleus in the cell has low deformability [18]. During passing through the gap, each cell shows deformation and rotation. Elongation of the cell tends to decrease the two-dimensional projected area of the cell facing the wall of the gap in the previous study [17]. Elongation of the cell tends to increase when the major axis is parallel to the flow direction of the medium fluid in the gap.

Outside the gap, the deformation direction ratio (*D*) fluctuates between 0 and 0.1, which corresponds to elongation to the flow direction (Fig. 4d). In the gap between 800 μm to 1000 μm, the deformation direction ratio (*D*) varies between – 0.1 and 0.1. In the gap, the deformation direction ratio (*D*) becomes negative sometimes, which corresponds to elongation to the direction perpendicular to the flow.

In the present study, the two-dimensional projected area tends to approach a circle as the cell deforms within the gap. A cell tends to extend in the direction of flow in the gap (Fig. 6b). The designed micro gap can be used to analyze the mechanism of deformation of the single biological cell to pass through the gap.

5. CONCLUSIONS

The alignment of a cell deformation during passing through the micro gap has been studied using the micro gap between the ridge and the groove manufactured in the micro flow channel by photolithography technique. During the movement of passing through the gap, the myoblast cell tends to extend in the direction of flow with the increase of the velocity.

ACKNOWLEDGMENT

The authors thank Dr. Yusuke Takahashi, Mr. Yuki Takiguchi and Shoki Toyota for their help of the experiment.

REFERENCES

[1] I. Safeukui, P.A. Buffet, G. Deplaine, S. Perrot, V. Brousse, A. Sauvanet, B. Aussilhou, S. Dokmak, A. Couvelard, D. Cazals-Hatem, O. Mercereau-Puijalon, G. Milon, P.H. David and N. Mohandas, "Sensing of Red Blood Cells with Decreased Membrane Deformability by the Human Spleen", **Blood Advances**, Vol. 2, No. 20, 2018, pp. 2581-2587.

[2] S. Hashimoto, "Detect of Sublethal Damage with Cyclic Deformation of Erythrocyte in Shear Flow", **Journal of Systemics Cybernetics and Informatics**, Vol. 12, No. 3, 2014, pp. 41-46.

[3] S. Hashimoto, "Applications of Polydimethylsiloxane: Microstructure of Functional Surface for Observation of Biological Cell Behavior", P.N. Carlsen ed., **Polydimethylsiloxane: Structure and Applications**, New York: Nova Science Pub. Inc., 2020, pp. 29-94.

[4] S. Hashimoto, T. Matsumoto, S. Uehara, "How Does a Cell Change Flow Direction Due to a Micro Groove?", **Journal of Systemics Cybernetics and Informatics**, Vol. 19, No. 8, 2021, pp. 164-181.

[5] Z. Chen, T.F. Yip, Y. Zhu, J.W.K. Ho and H. Chen, "The Method to Quantify Cell Elasticity Based on the Precise Measurement of Pressure Inducing Cell Deformation in Microfluidic Channels", **Methods X**, Vol. 8, 2021, 101247, pp. 1-9.

[6] J.E. Shim, J. Bu, M.K. Lee, Y.H. Cho, T.H. Kim, J.U. Bu and S.W. Han, "Viable and High-throughput Isolation of Heterogeneous Circulating Tumor Cells Using Tapered-slit Filters", **Sensors and Actuators B: Chemical**, Vol. 321, 2020, 128369, pp. 1-8.

[7] A. Mirzaaghaian, A. Ramiar, A.A. Ranjbar and M.E. Warkiani, "Application of Level-set Method in Simulation of Normal and Cancer Cells Deformability within a Microfluidic Device", **Journal of Biomechanics**, Vol. 112, 2020, 110066, pp. 1-9.

[8] S.J. Hymel, H. Lan and D.B. Khismatullin, "Elongation Index as a Sensitive Measure of Cell Deformation in High-Throughput Microfluidic Systems", **Biophsycal Journal**, Vol. 119, No. 3, 2020, pp. 493-501.

[9] M. Hakim, F. Khorasheh, I. Alemzadeh and M. Vossoughi, "A New Insight to Deformability Correlation of Circulating Tumor Cells with Metastatic Behavior by Application of a New Deformability-based Microfluidic Chip", **Analytica Chimica Acta**, Vol. 1186, 2021, 339115, pp. 1-8.

[10] F.J. Armistead, J.G. De Pablo, H. Gadêlha, S.A. Peyman and S.D. Evans, "Cells Under Stress: An Inertial-shear Microfluidic Determination of Cell Behavior", **Biophsycal Journal**, Vol. 116, No. 6, 2019, pp. 1127-1135.

[11] Y. Takahashi, S. Hashimoto, H. Hino and T. Azuma, "Design of Slit between Micro Cylindrical Pillars for Cell Sorting", **Journal of Systemics, Cybernetics and Informatics**, Vol. 14, No. 6, 2016, pp. 8-14.

[12] S. Hashimoto, "Micro Machined Slit between Ridge And Groove in Micro Fluid-channel to Measure Floating Cell Deformability", **Proceedings of the ASME 2020 Fluids Engineering Division Summer Meeting (FEDSM2020)**, 2020, pp. 1-7.

[13] Y. Takahashi, S. Hashimoto, A. Mizoi and H. Hino, "Deformation of Cell Passing through Micro Slit between Micro Ridges Fabricated by Photolithography Technique", **Journal of Systemics Cybernetics and Informatics**, Vol. 15, No. 3, 2017, pp. 1-9.

[14] A.R. Bausch, W. Moeller and E. Sackmann, "Measurement of Local Viscoelasticity and Forces in Living Cells by Magnetic Tweezers", **Biophysical Journal**, Vol. 76, No. 1, 1999, pp. 573-579.

[15] S.E Cross, Y.-S. Jin, J. Tondre, R. Wong, J.Y. Rao and J.K. Gimzewski, "AFM-based Analysis of Human Metastatic Cancer Cells", **Nanotechnology**, Vol. 19, No. 38, 2008, 384003, pp.1-8.

[16] G. Bao and S. Suresh, "Cell and Molecular Mechanics of Biological Materials", **Nature Materials**, Vol. 2, No. 11, 2003, pp. 715-725.

[17] B. Lincoln, H.M. Erickson, S. Schinkinger, F. Wottawah, D. Mitchell, S. Ulvick, C. Bilby and J. Guck, "Deformability-Based Flow Cytometry", **Cytometry**, Part A: the journal of the International Society for Analytical Cytology, Vol. 59, No.2, 2004, pp. 203-209.

[18] S. Uehara, S. Hashimoto, "How Does Cell Deform during Movement in Micro Gap?", **Proc. 25th World Multi-Conference on Systemics Cybernetics and Informatics**, Vol. 3, 2021, pp. 72-77.

[19] E. Antmen, U. Demirci and V. Hasirci, "Amplification of Nuclear Deformation of Breast Cancer Cells by Seeding on Micropatterned Surfaces to Better Distinguish Their Malignancies", **Colloids and Surfaces B: Biointerfaces**, Vol. 183, 2019, 110402, pp. 1-12.